Strong in-plane anisotropy in the electronic structure of fixed-valence β-$LuAlB_4$

Pascal Reiss,[1,2,*] Jordan Baglo,[1,†] Hong'En Tan,[1,3] Xiaoye Chen,[1] Sven Friedemann,[4] Kentaro Kuga,[5,‡] F. Malte Grosche,[1] Satoru Nakatsuji,[5,6,7,8] and Michael Sutherland[1,§]

[1] *Cavendish Laboratory, University of Cambridge, Cambridge, CB3 0HE, United Kingdom*
[2] *Clarendon Laboratory, University of Oxford, Oxford, OX1 3PU, United Kingdom*
[3] *Complex Systems Group, Institute of High Performance Computing, A*STAR, Singapore, 138632*
[4] *HH Wills Laboratory, University of Bristol, Bristol, BS8 1TL, United Kingdom*
[5] *Institute for Solid State Physics, University of Tokyo, Kashiwa 277-8581, Japan*
[6] *CREST, Japan Science and Technology Agency, Kawaguchi, Saitama 332-0012, Japan*
[7] *Department of Physics, University of Tokyo, Bunkyo-ku, Tokyo 113-0033, Japan*
[8] *Trans-scale Quantum Science Institute, University of Tokyo, Bunkyo-ku, Tokyo 113-0033, Japan*

(Dated: July 10, 2020)

The origin of intrinsic quantum criticality in the heavy-fermion superconductor β-$YbAlB_4$ has been attributed to strong Yb valence fluctuations and its peculiar crystal structure. Here, we assess these contributions individually by studying the isostructural but fixed-valence compound β-$LuAlB_4$. Quantum oscillation measurements and DFT calculations reveal a Fermi surface in β-$LuAlB_4$ markedly different from that of β-$YbAlB_4$, consistent with a 'large' Fermi surface in the latter. We also find an unexpected in-plane anisotropy of the electronic structure, in contrast to the isotropic Kondo hybridization in β-$YbAlB_4$.

At a quantum critical point (QCP), a continuous, zero-temperature phase transition occurs when the ordered and disordered phases are energetically degenerate. Usually, this requires tuning materials to some material-dependent critical pressure, composition or magnetic field [1]. However, there are rare cases where quantum critical phenomena can be observed without tuning. Studying such 'intrinsic' quantum criticality aims at identifying robust mechanisms for unusual electronic phases, raising the prospect of unconventional superconductivity [2, 3].

The heavy-fermion superconductor β-$YbAlB_4$ is an example for such an intrinsically quantum critical system [4]. Initial evidence for its non-accidental nature was the observation of quantum critical behavior in this stoichiometric, clean system at zero magnetic field, which was later extended to finite pressures, providing an example for a quantum critical phase [5, 6]. Transport and thermodynamic measurements identified non-Fermi liquid behavior, yet the Wiedemann-Franz law is obeyed, demonstrating that quasiparticles remain intact [4, 7, 8].

It was realised that the peculiar crystal environment of the Yb atoms, as well as strong Yb valence fluctuations are central for understanding the physics of β-$YbAlB_4$ [9–11]. The material crystallizes into the orthorhombic $ThMoB_4$ structure where a distorted honeycomb lattice of Yb and Al atoms is sandwiched between layers of B atoms. As shown in Fig. 1, the B atoms occupy independent sites B1–B3, which give rise to a network of five- and sevenfold boron rings [12]. The Kondo hybridization induced by the orbital overlap within the Yb-B-ring structure was argued to be strongly anisotropic between the crystal c axis and the (ab) plane, but *isotropic* within the (ab) plane [13]. This hybridization can induce the observed T/B scaling of the magnetic susceptibility, and can also explain the intrinsic quantum criticality in β-$YbAlB_4$ [5, 13–18]. Recently, strong evidence supporting the in-plane isotropy was found in the linear dichroism of core-level x-ray photoemission and NMR studies [19, 20].

The isomorph α-$YbAlB_4$ features the same local symmetry and similar valence fluctuations of the Yb atoms, as well as an essentially identical in-plane isotropy of the Kondo hybridization [9, 12, 19, 21]. However, it does not show superconductivity nor intrinsic quantum criticality [12]. This indicates that the effect of the lattice cannot be truncated to the local environment of the Yb atoms, and/or that subtle differences in the Yb-B structures between α- and β-$YbAlB_4$ are pivotal [20, 21].

It is therefore paramount to assess the importance of the lattice structure in detail [22, 23]. For this purpose, β-$LuAlB_4$ is ideally suited, as it crystallizes into the same structure as β-$YbAlB_4$, with nearly identical lattice parameters [12, 24]. The Lu $4f$ states are fully occupied and fall well below the Fermi level. Thus, the electronic structure of β-$LuAlB_4$ represents the 'small' Fermi surface limit of β-$YbAlB_4$, and the Kondo effect and valence fluctuations are suppressed.

In this Rapid Communication, we investigate the electronic structure of β-$LuAlB_4$ using Shubnikov-de Haas oscillation measurements. We resolve all Fermi surface sheets predicted by DFT calculations and we extract the charge carrier masses. Our findings are broadly consistent with DFT predictions, validating a closer look at the electronic structure in real space. This reveals that the Lu-B hybridization and the charge distribution in the unit cell are strongly *anisotropic*, in contrast to the *isotropic* Kondo hybridization in β-$YbAlB_4$.

Using the Al flux method [12], thin ($d \lesssim 10\,\mu m$), platelike single crystals of β-$LuAlB_4$ were grown, with the crystal c axis normal to the plates, confirmed by X-ray diffraction measurements. For the resistivity mea-

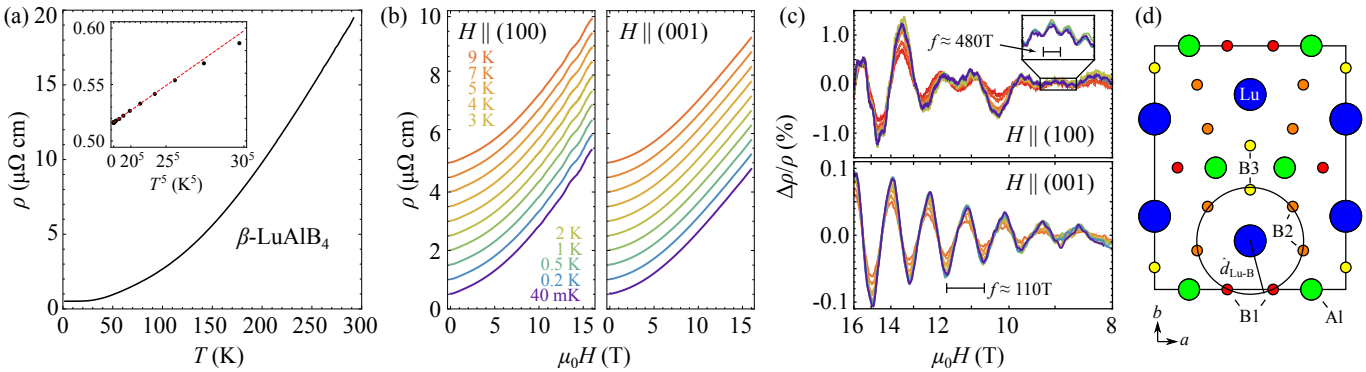

FIG. 1. (a) Temperature and (b) magnetic field dependence of the electrical resistivity of single-crystalline β-$LuAlB_4$. The insert shows the low-temperature resistivity against T^5, and the red dashed line is a linear fit below 25 K. Data in (b) are vertically offset for clarity. (c) Background subtracted data plotted against inverse field $1/H$. The periodic oscillations in $\Delta\rho/\rho(T)$ are clearly seen. (d) A 2D projection of the crystal structure. The seven-fold B ring is highlighted, consisting of atomic sites B1-B3. The average Lu-B distance is given as $\hat{d}_{\text{Lu-B}}$ which shows small variations, most pronounced for B3 [12].

surements, we used a standard four contact setup with $I < 1$ mA in the (ab) plane. Contacts were spot-welded and fixed with DuPont 6838 silver epoxy. The irregular shape of the brittle samples and a large relative uncertainty in the sample thickness put constraints on the contact layout and the determination of absolute values of the resistivity. Several samples were screened using a Quantum Design PPMS, and the best sample with a residual resistivity ratio RRR= 34 was used for all experiments. Quantum oscillation experiments were conducted using an 18 T dilution refrigerator in Cambridge equipped with low-temperature transformers. Two sets of measurements were performed, spanning sample rotations by almost 90° with the magnetic field ranging from the crystal (001) axis to the (100) and to the (010) axis.

Band structure calculations were carried out using density functional theory, linear augmented plane waves and the PBE generalised gradient approximation as implemented in WIEN2k [25, 26]. Relativistic local orbits and spin-orbit coupling were included. Small Fermi surface pockets were resolved using 100,000 k-points in the Brillouin zone. $RK_{\mathbf{max}}$ was set to 7.0, and experimental lattice parameters and atomic positions were used [12]. Fermi surfaces were plotted using XCrySDen, and extremal orbits extracted using SKEAF [27, 28].

In Figure 1(a), we show the sample resistivity $\rho(T)$ as a function of temperature T. Good metallic behavior is found, and no phase transitions including superconductivity could be identified above $T \approx 40$ mK, in agreement with previous reports [12]. The small residual resistivity $\rho_0 \approx 0.5\,\mu\Omega$ cm in the zero-temperature limit suggests large carrier densities and/or mobilities. As shown in the inset of Fig. 1(a), $\rho(T)$ shows a marked T^5 dependence below $T \approx 25$ K. This demonstrates that electron-electron interactions are not dominating the quasiparticle scattering in this regime, in contrast to (non-critical) strongly-correlated systems, where electron-electron scattering leads to a Fermi liquid T^2 behavior. The T^5 dependence is an indicator for dominant quasi-elastic electron-phonon scattering instead.

In order to determine the electronic structure in detail, we performed Shubnikov-de Haas measurements up to $\mu_0 H = 18$ T as a function of temperature and field orientation. A selection of magnetoresistivity curves is shown in Fig. 1(b) which demonstrate that the magnetoresistivity is essentially temperature-independent over more than two decades up to $T \approx 9$ K. This observation suggests that quasiparticle mobilities and densities remain constant in this temperature regime, which is consistent with the effectively constant zero-field resistivity below $T \approx 10$ K, Fig. 1(a). However, this observation is in marked contrast to β-$YbAlB_4$ where a nearly 80 % decrease in mobilities was found below 10 K upon approaching the quantum critical point [31].

From Fig. 1(b), and in particular for $H||(100)$, a strong oscillatory component of the high-field resistivity can be seen [30]. On one hand, the large amplitudes of these quantum oscillations demonstrate the high quality of the sample studied. On the other hand, the oscillations remain visible even for $T = 9$ K, suggesting small quasiparticle masses m, equivalent to large mobilities $|\mu| \sim 1/m$.

We now turn to a quantitative analysis of these quantum oscillations. In Fig. 1(c), a smooth, low-order polynomial background has been removed. When plotted against $1/H$, multiple frequencies f are apparent, which correspond to extremal cross-sectional areas A of the Fermi surface perpendicular to the magnetic field [30] $f = A\hbar/(2\pi e)$. We employ an FFT, shown in Fig. 2(a), to extract the oscillation frequencies and amplitudes as a function of temperature and field orientation (see also the Supplemental Material (SM) [29]). All obtained frequencies are shown in Fig. 2(b) on top of the FFT spectra, represented as a background color scale. We identify a set of branches for fields close to the (010) direc-

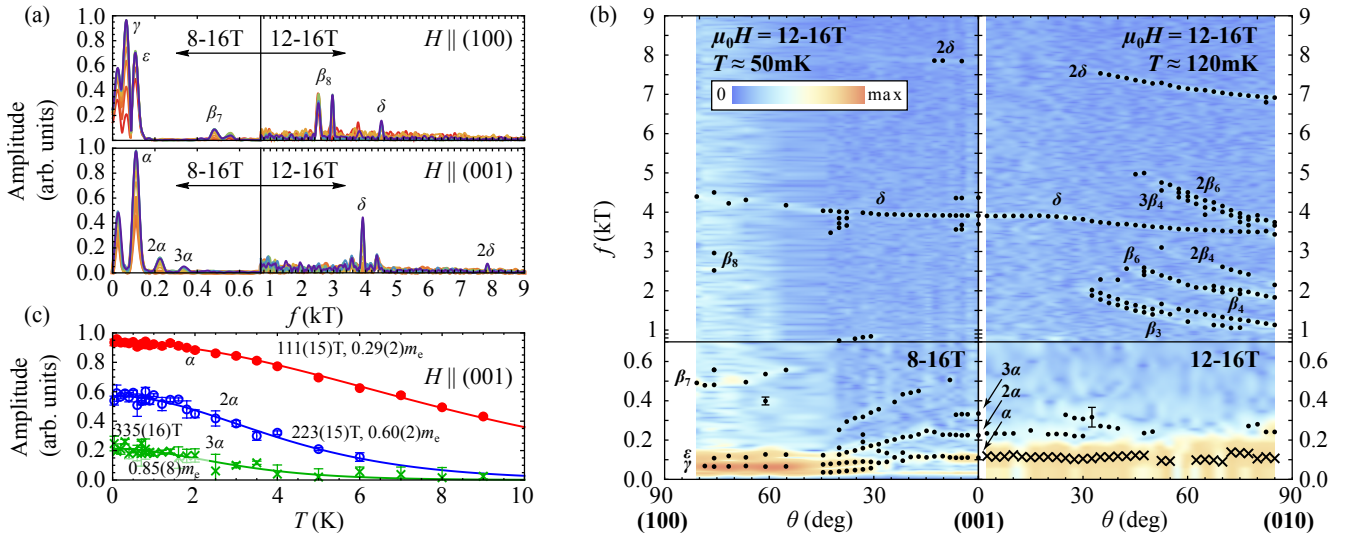

FIG. 2. Quantum oscillations in β-LuAlB$_4$. (a) FFT spectra for two field orientations, showing a range of peaks. The field ranges chosen serve to maximize the visibility of the high and low frequency peaks. (b) Angular dependence of the FFT spectral intensity shown as a color map. Extracted peak positions are shown as black dots, and frequencies extracted from direct fits are shown as black crosses (cf. Ref. 29). Representative error bars show the FFT peak FWHM. For $f \geq 0.7\,\mathrm{kT}$, they are smaller than the symbol size. (c) Temperature dependence of the α, 2α and 3α oscillation amplitude (points), and a fit to the Lifshitz-Kosevich form (lines) [30]. Error bars and values denote a 1σ confidence interval.

tion, labelled β_{3-6}. These branches display an approximate $1/\sin(\theta)$ dependence, where θ measures the angle away from (001). Such a dependence is consistent with a weakly warped two-dimensional Fermi surface pocket along the reciprocal b axis. Next, we find two weakly orientation-dependent lines for $3.4\,\mathrm{kT} \leq f \leq 4.5\,\mathrm{kT}$ and $f \geq 6.8\,\mathrm{kT}$ which we call δ and 2δ. Their flat dependencies are consistent with nearly spherical Fermi surface pockets, however the integer ratio between their frequencies suggests that 2δ is the first harmonic of δ. Finally, multiple frequencies below 0.9 kT are found with no obvious analytical dependence, labelled α, γ, ϵ and β_7.

Next, cyclotron masses are extracted by following the oscillation amplitudes as a function of temperature, as shown in Fig. 2(c). Fitting the Lifshitz-Kosevich form [30], we find $m \approx 0.29 m_e$ for α, which is much smaller than any cyclotron mass reported on the more strongly correlated β-YbAlB$_4$ [32]. The integer ratios between the frequencies and masses of orbits α, 2α and 3α allow us to identify α as a fundamental frequency, and 2α and 3α as harmonics. Further orbits are discussed in the SM [29]. For the following discussion, we will omit harmonics identified in this way, as summarised in Fig. 3(c).

To better understand the observed quantum oscillations, we now turn to our DFT calculations. In Fig. 3(a), we show the computed band structure and density of states (DOS) over a wide energy range. The localized Lu $4f$ states are easily identified about 4.1 eV and 5.6 eV below the Fermi level E_F. In the vicinity of E_F, the DOS is dominated by Lu and B states whereas the Al states play a minor role. Two bands cross the Fermi level, which give rise to two Fermi surface sheets with equal volume, one hole-like and one electron-like, as shown in Fig. 3(b). The hole-like sheet consists of two strongly warped cylinders along (010) which give rise to the extremal orbits β_{1-8}. They are joined by two three-dimensional pockets, producing orbits α_{1-3}. The electron-like sheet consists of nearly spherical pockets in the corners of the first Brillouin zone which are the origin of the orbit δ. Further pockets with varying sizes surround the Γ point, with orbits labelled γ_{1-3} and ϵ.

In Fig. 3(c), we compare the computed extremal Fermi surface cross-sections translated into quantum oscillation frequencies to the experimentally determined fundamental frequencies. The agreement is convincing: the line δ and the branches β_{3-6} are reproduced, and most frequencies below 0.9 kT can be mapped within experimental resolution ($\Delta f \approx 40 - 100\,\mathrm{T}$ FWHM depending on field range). DFT slightly underestimates the size of the large Fermi surface pockets, i.e. predicted frequencies are slightly smaller than observed ones, as evident from Fig. 3(c). This applies to both electron-like and hole-like bands, consistent with an overall charge balance.

Having determined the electronic structure of β-LuAlB$_4$, the isostructural but fixed-valence reference compound to β-YbAlB$_4$, we now discuss the two main implications of the findings. Firstly, the frequencies of the quantum oscillations and their angular dependence, as well as the cyclotron masses reported here differ greatly from results on β-YbAlB$_4$ studied previously [32]. The most notable difference is the absence of the spherical pocket δ in β-YbAlB$_4$. Conversely, large cross-

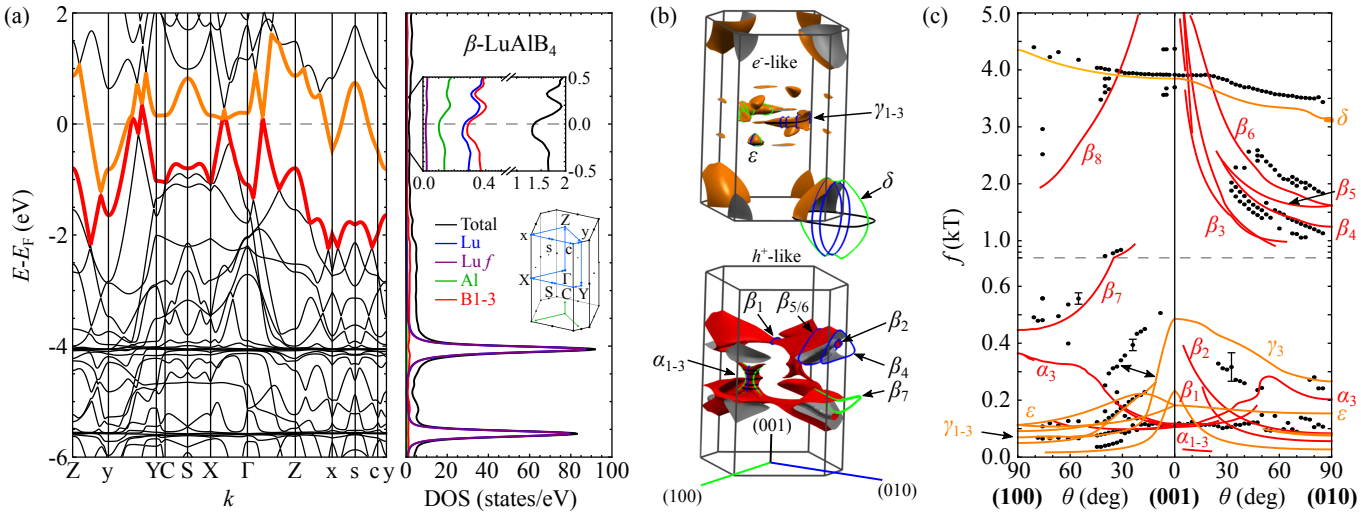

FIG. 3. DFT simulations and comparison to experiment. (a) Band structure and density of states (DOS). Insets show the magnified DOS at the Fermi level and the path in k space. (b) Fermi surface sheets corresponding to bands crossing the Fermi level. Orbits around extremal cross sections are shown for field directions along the reciprocal axes (color coding as shown). (c) Comparison of predicted frequencies (lines) with extracted fundamental ones (dots). Error bars are defined as in Fig. 2.

sectional areas were observed in β-YbAlB$_4$ (dubbed β in Ref. 32), which have no counterpart in β-LuAlB$_4$. Such substantial differences in the Fermi surface suggest that in the presence of large magnetic fields, the Fermi surface of β-YbAlB$_4$ is not 'small' but 'large' and the $4f$ hole is delocalized [32]. Moreover, the experimental cyclotron masses of β-LuAlB$_4$ are in good agreement with predicted values (Table SMI [29]), but they are on average a factor 10 smaller than in β-YbAlB$_4$ [32]. This reflects the significant mass enhancement due to the presence of correlated f-states near the Fermi energy.

The second implication is most evident from the hole-like Fermi surface sheet of β-LuAlB$_4$, Fig. 3(b): There is a strong anisotropy of the electronic structure within the (ab) plane. To trace its origin, we reiterate that the DOS at the Fermi level E_F has predominant Lu and B character, as shown in Fig. 3(a). It is therefore suggestive to attribute the anisotropy to the Lu-B hybridization. This is confirmed when returning to real space: in Fig. 4(a) and (b), we show the computed charge distribution in the unit cell for states close to E_F. We find a much larger orbital overlap between the Lu d_{z^2} and the B3 p_z states, when compared to B1 and B2. A similar result is obtained when comparing the contributions of the B atoms to the DOS, Fig. 4(c). Over a wide energy range around E_F, the B3 states contribute roughly 30% more than B1 and B2, which originates fully from their p_z orbitals.

This inequivalence of the B atoms cannot be assigned to the form of the aforementioned atomic orbitals, since B p_z and Lu d_{z^2} orbitals are rotationally invariant along the crystal c axis. Hence, no anisotropy is expected for an isolated stack of Lu atoms and ideal B rings. Consequently, we must link it to the variation in Lu-B bond lengths (where the Lu-B3 bond is the shortest), and/or the global charge distribution within the orthorhombic unit cell. As shown in Fig. 4(b), the charge carrier density is indeed strongly anisotropic: it is the largest within the Lu-B3-B3-Lu structure along the crystal b axis, whereas the B1 and B2 atoms can be projected onto low-density stripes. The Al sites are effectively disconnected from charge carriers occupying states close to E_F which marks them as ideally suited for chemical doping minimizing quasiparticle scattering.

We conclude by discussing the implications on β-YbAlB$_4$. As it is isostructural to β-LuAlB$_4$, and since the Lu/Yb-B bond length variations are nearly identical (4.0% in critical β-YbAlB$_4$ and 3.8% in non-critical β-LuAlB$_4$, in contrast to 5.1% in non-critical α-YbAlB$_4$ [12]), we would expect that a similarly anisotropic orbital overlap should prevail in β-YbAlB$_4$ (see also the SM for a detailed comparison [29]). However, previous studies in quantum critical α- and β-YbAlB$_4$ found a Kondo hybridization which is isotropic in the (ab) plane [19, 20]. Our finding therefore provides evidence that the *isotropic* Kondo hybridization and intrinsic quantum criticality in β-YbAlB$_4$ emerge from an *anisotropic* electronic structure [9, 10, 16, 21]. Identifying a mechanism which counteracts this electronic anisotropy and/or (self-)stabilizes the quantum critical phase remains an open problem.

Acknowledgements. We thank Swee K. Goh for experimental assistance, and Hisatomo Harima for insightful discussions. PR acknowledges support from the Cusanuswerk (Germany) and the Oxford Quantum Materials Platform Grant (EPSRC No. EP/M020517/1). SF, FMG and MS acknowledge support from EPSRC Grants No. EP/N026691/1 and EP/K012894/1. This work is partially supported by Grants-in-Aids for Scientific Research on Innovative Areas (15H05882 and 15H05883),

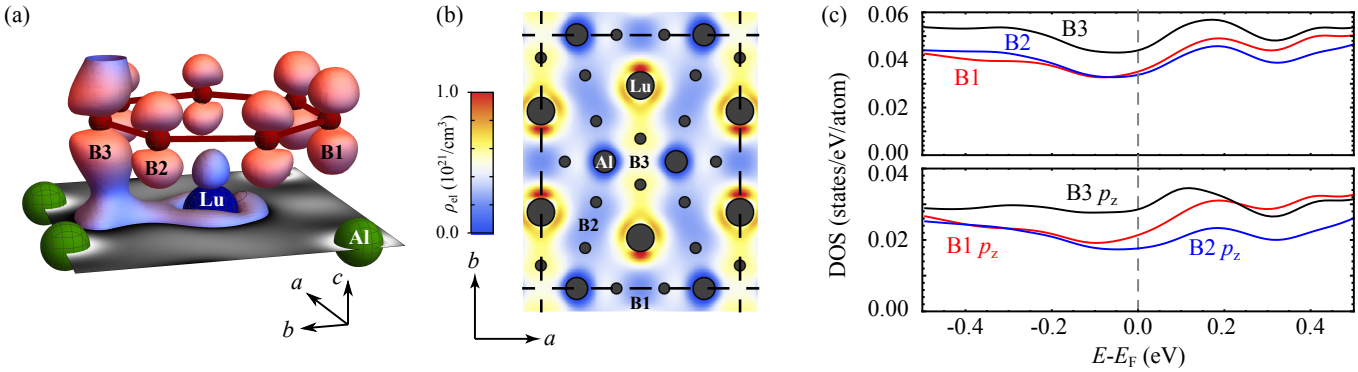

FIG. 4. Inequivalence of the boron atoms. (a) Charge carrier distribution ρ_{el} in the proximity of the Lu atom and the sevenfold B ring. Electronic states within $\Delta E = k_B \cdot 300\,\mathrm{K}$ of the Fermi level were included. The closed surfaces encapsulate regions with $\rho_{el} > 0.55 \cdot 10^{21}/\mathrm{cm}^3$. (b) The charge carrier distribution in the Lu/Al layer of the unit cell, with the B atoms projected. (c) Comparison of the density of states contributions of the B atoms. Upper panel: total contribution, lower panel: p_z states only.

by Grants-in-Aid for Scientific Research (19H00650) from JSPS, and by CREST (JPMJCR18T3), Japan Science and Technology Agency (JST). Access to experimental data will be provided at [33].

* pascal.reiss@physics.ox.ac.uk
† Current address: Institut Quantique, Département de Physique & RQMP, Université de Sherbrooke, Sherbrooke, Québec J1K 2R1, Canada
‡ Current address: Toyota Technological Institute, Nagoya, 468-8511, Japan
§ mls41@cam.ac.uk

[1] H. von Löhneysen, A. Rosch, M. Vojta, and P. Wölfle, Fermi-liquid instabilities at magnetic quantum phase transitions, Reviews of Modern Physics **79**, 1015 (2007).
[2] I. Esterlis and J. Schmalian, Cooper pairing of incoherent electrons : An electron-phonon version of the Sachdev-Ye-Kitaev model, Physical Review B **100**, 115132 (2019).
[3] D. Hauck, M. J. Klug, I. Esterlis, and J. Schmalian, Eliashberg equations for an electron – phonon version of the Sachdev – Ye – Kitaev model : Pair breaking in non-Fermi liquid superconductors, Annals of Physics , 168120 (2020).
[4] S. Nakatsuji, K. Kuga, Y. Machida, T. Tayama, T. Sakakibara, Y. Karaki, H. Ishimoto, S. Yonezawa, Y. Maeno, E. Pearson, G. G. Lonzarich, L. Balicas, H. Lee, and Z. Fisk, Superconductivity and quantum criticality in the heavy-fermion system β-YbAlB$_4$, Nature Physics **4**, 603 (2008).
[5] Y. Matsumoto, S. Nakatsuji, K. Kuga, Y. Karaki, N. Horie, Y. Shimura, T. Sakakibara, A. H. Nevidomskyy, and P. Coleman, Quantum criticality without tuning in the mixed valence compound β-YbAlB$_4$., Science **331**, 316 (2011).
[6] T. Tomita, K. Kuga, Y. Uwatoko, P. Coleman, and S. Nakatsuji, Strange metal without magnetic criticality, Science **349**, 506 (2015).
[7] S. Nakatsuji, K. Kuga, T. Tomita, and Y. Matsumoto, Pronounced non-Fermi-liquid behavior of the quantum critical heavy fermion superconductor β-YbAlB$_4$, Physica Status Solidi (B) **247**, 485 (2010).
[8] M. L. Sutherland, E. C. T. O'Farrell, W. H. Toews, J. Dunn, K. Kuga, S. Nakatsuji, Y. Machida, K. Izawa, and R. W. Hill, Intact quasiparticles at an unconventional quantum critical point, Physical Review B **92**, 041114(R) (2015).
[9] M. Okawa, M. Matsunami, K. Ishizaka, R. Eguchi, M. Taguchi, A. Chainani, Y. Takata, M. Yabashi, K. Tamasaku, Y. Nishino, T. Ishikawa, K. Kuga, N. Horie, S. Nakatsuji, and S. Shin, Strong valence fluctuation in the quantum critical heavy fermion superconductor β-YbAlB$_4$: A hard x-ray photoemission study, Physical Review Letters **104**, 247201 (2010).
[10] S. Watanabe and K. Miyake, Quantum Valence Criticality as an Origin of Unconventional Critical Phenomena, Physical Review Letters **105**, 186403 (2010).
[11] A. H. Nevidomskyy and P. Coleman, Layered Kondo Lattice Model for Quantum Critical β-YbAlB$_4$, Physical Review Letters **102**, 077202 (2009).
[12] R. T. Macaluso, S. Nakatsuji, K. Kuga, E. L. Thomas, Y. Machida, Y. Maeno, Z. Fisk, and J. Y. Chan, Crystal Structure and Physical Properties of Polymorphs of LnAlB$_4$ (Ln = Yb, Lu), Chemistry of Materials **19**, 1918 (2007).
[13] A. Ramires, P. Coleman, A. H. Nevidomskyy, and A. M. Tsvelik, β-YbAlB$_4$: A Critical Nodal Metal, Physical Review Letters **109**, 176404 (2012).
[14] L. M. Holanda, J. M. Vargas, W. Iwamoto, C. Rettori, S. Nakatsuji, K. Kuga, Z. Fisk, S. B. Oseroff, and P. G. Pagliuso, Quantum Critical Kondo Quasiparticles Probed by ESR in β-YbAlB$_4$, Physical Review Letters **107**, 026402 (2011).
[15] S. Watanabe and K. Miyake, Quantum criticality and emergence of the T/B scaling in strongly correlated metals, Journal of Magnetism and Magnetic Materials **400**, 13 (2016).
[16] S. Watanabe and K. Miyake, Charge Transfer Effect under Odd-Parity Crystalline Electric Field: Divergence of Magnetic Toroidal Fluctuation in β-YbAlB$_4$, Journal of the Physical Society of Japan **88**, 033701 (2019).
[17] A. Ramires and P. Coleman, Theory of the Electron Spin Resonance in the Heavy Fermion Metal β-YbAlB$_4$, Physical Review Letters **112**, 116405 (2014).

[18] Y. Komijani and P. Coleman, Model for a Ferromagnetic Quantum Critical Point in a 1D Kondo Lattice, Physical Review Letters **120**, 157206 (2018).

[19] K. Kuga, Y. Kanai, H. Fujiwara, K. Yamagami, S. Hamamoto, Y. Aoyama, A. Sekiyama, A. Higashiya, T. Kadono, S. Imada, A. Yamasaki, A. Tanaka, K. Tamasaku, M. Yabashi, T. Ishikawa, S. Nakatsuji, and T. Kiss, Effect of Anisotropic Hybridization in $YbAlB_4$ Probed by Linear Dichroism in Core-Level Hard X-Ray Photoemission Spectroscopy, Physical Review Letters **123**, 036404 (2019).

[20] S. Takano, M. S. Grbic, K. Kimura, M. Yoshida, M. Takigawa, E. C. Farrell, K. Kuga, S. Nakatsuji, and H. Harima, Site-selective ^{11}B NMR studies on $YbAlB_4$, Journal of Physics: Conference Series **683** (2016).

[21] K. Kuga, Y. Matsumoto, M. Okawa, S. Suzuki, T. Tomita, K. Sone, Y. Shimura, T. Sakakibara, D. Nishio-Hamane, Y. Karaki, Y. Takata, M. Matsunami, R. Eguchi, M. Taguchi, A. Chainani, S. Shin, K. Tamasaku, Y. Nishino, M. Yabashi, T. Ishikawa, and S. Nakatsuji, Quantum valence criticality in a correlated metal, Science Advances **4**, eaao3547 (2018).

[22] S. Friedemann, S. K. Goh, P. M. C. Rourke, P. Reiss, M. L. Sutherland, F. M. Grosche, G. Zwicknagl, and Z. Fisk, Electronic structure of $LuRh_2Si_2$: 'small' Fermi surface reference to $YbRh_2Si_2$, New Journal of Physics **15**, 093014 (2013).

[23] P. Reiss, P. M. C. Rourke, G. Zwicknagl, F. M. Grosche, and S. Friedemann, $LuRh_2Si_2$: Sensitivity of the Fermi surface to the Si z-position, physica status solidi (b) **250**, 498 (2013).

[24] M. Seitz, A. G. Oliver, and K. N. Raymond, The Lanthanide Contraction Revisited, Journal of the American Chemical Society **129**, 11153 (2007).

[25] J. P. Perdew, K. Burke, and M. Ernzerhof, Generalized Gradient Approximation Made Simple, Physical Review Letters **77**, 3865 (1996).

[26] K. Schwarz and P. Blaha, Solid state calculations using WIEN2k, Computational Materials Science **28**, 259 (2003).

[27] A. Kokalj, XCrySDen, `http://www.xcrysden.org/`.

[28] P. M. C. Rourke and S. R. Julian, Numerical extraction of de Haas – van Alphen frequencies from calculated band energies, Computer Physics Communications **183**, 324 (2012).

[29] See Supplemental Material at [URL will be inserted by publisher] for further field measurements and analyses, and a summary table.

[30] D. Shoenberg, *Magnetic oscillations in metals* (Cambridge University Press, Cambridge, 1984).

[31] E. C. T. O'Farrell, Y. Matsumoto, and S. Nakatsuji, Evolution of c-f hybridization and two-component hall effect in β-$YbAlB_4$, Physical Review Letters **109**, 176405 (2012).

[32] E. C. T. O'Farrell, D. A. Tompsett, S. E. Sebastian, N. Harrison, C. Capan, L. Balicas, K. Kuga, A. Matsuo, K. Kindo, M. Tokunaga, S. Nakatsuji, G. Csányi, Z. Fisk, and M. L. Sutherland, Role of f Electrons in the Fermi Surface of the Heavy Fermion Superconductor β-$YbAlB_4$, Physical Review Letters **102**, 216402 (2009).

[33] URL will be created.